
Proceedings of the Seventeenth International Conference on
Civil, Structural and Environmental Engineering Computing
Edited by: P. Iványi, J. Kruis and B.H.V. Topping
Civil-Comp Conferences, Volume 6, Paper 3.3
Civil-Comp Press, Edinburgh, United Kingdom, 2023
doi: 10.4203/ccc.6.3.3


# A Small-Strain Damping Model for Gravelly Soils subjected to Different Excitation Frequencies

**Q.Z. Sang[1], X. Chen[2] and Y. Yuan[1,3]**

**[1]College of Civil Engineering, Tongji University, Shanghai, China**
**[2]College of Civil Engineering and Architecture, Jiaxing University, Zhejiang, China**
**[3]State-Key Laboratory of Disaster Prevention in Civil Engineering, Shanghai, China**

## Abstract

In order to account for hydraulic damping in liquefiable areas, a small-strain damping model in shear for gravelly soil subjected to different loading frequencies was presented. The total damping was decomposed into skeleton damping and hydraulic damping induced by motion of viscous pore fluid relative to skeleton. The former was represented by an empirical expression while the latter term was obtained based on Biot theory. The fitting parameters were then determined by using Particle Swarm Optimization (PSO) algorithm. Results were found to match well with experimental data from torsional shear test for gravelly soils of various particle size distributions and under different isotropic confining pressures. Parametric analysis indicated that the hydraulic damping increases monotonically with rising mean grain size and loading frequency, whereas a critical grain size exists at which the total damping takes its minimum value under a given frequency.

**Keywords:** skeleton damping, hydraulic damping, Biot theory, particle swarm optimization, gravelly soils

## 1 Introduction

To ensure the safety of underground structures in earthquake prone areas, the seismic stability of structures must be tested. It should be noted, however, that the reliable

dynamic properties (including liquefaction resistance) of soils are prerequisites for use in seismic analysis of underground structures.

Pore fluid induced damping (hydraulic damping) is generally negligible in current geotechnical engineering research, even in liquefiable areas. However, this assumption is found to be invalid for soils with high permeability (gravels) and high frequency excitations [1]. The hydraulic damping has been investigated in some work generally in resonant column tests, calculated by means of half-power bandwidth (HPB) and free vibration decay (FVD) methods. Investigations of saturation effects on damping cover sands [2–4], silts [5] as well as clayed soils [6,7]. The increase of damping was found with increasing moisture content and decreasing confining pressure, and the effects of moisture content are noticeable at low confining pressure [5,6]. Transparent soil, which is widely used to track the behaviors of natural saturated soil, has been studied in [8]. It is also found therein that dynamic damping is remarkably influenced by properties of pore fluid.

However, focuses of previous studies are mostly laid on qualitative descriptions from observations [3,4]. Theoretical studies on hydraulic damping include [1,9-10], in which the Biot flow subjected to compression and torsional waves was evaluated analytically. The effect of non-Poiseuille flow at high frequencies was incorporated in [11]. In their model, the hydraulic damping was indirectly calculated from the difference between total damping and skeleton damping, and the skeleton damping was considered as a constant therein for ease of calculation. The consideration of hydraulic damping for coarse sands and gravels was highlighted from parametric studies.

In this paper, a total damping model for gravelly soils in shear under different loading frequencies is presented. The total damping is decomposed into skeleton damping and hydraulic damping, represented by empirical and analytical expressions, respectively. The soils could be unsaturated by simplifying the air-water mixture into a homogeneous single fluid phase as in [1], and the fluid compressibility is revised by moisture content. However, since the effects of moisture content do not contribute to rotational motion subjected to torsional waves, they are considered as a separated multiplier in the hydraulic damping herein. Key parameters affecting skeleton damping and hydraulic damping are explicitly incorporated with fitting parameters. In the following sections, the damping model was first reviewed, followed by the determination of fitting parameters through Particle Swarm Optimization (PSO) algorithm. Results were subsequently compared to experimental data from torsional shear test. Finally, parametric study was carried out to illustrate the effects of median grain size, effective stress and loading frequency on the damping.

## 2 Assumptions and Damping Model

In the presented model, several assumptions are made: (i) measurements in shear of soil are performed in linear range (this implies small-strain) with varying excitation

frequencies. That is, damping is of the minimum value, and the linear constitutive law is applied to solid skeleton; (ii) only the low frequency response in Biot model is involved, i.e., the pore fluid follows the Poiseuille flow. The low frequency bound of Biot media is distinguished by a characteristic frequency

$$f_c = ng/2\pi k, \tag{1}$$

where, $n$ and $k$ denote the porosity and hydraulic conductivity respectively, and $g$ is the acceleration of gravity.

Under the above assumptions, the total small-strain damping of Biot media in shear could be decomposed into skeleton damping and hydraulic damping induced by Biot flow, which is expressed as

$$D_{min,s} = D_s + D_f, \tag{2}$$

where $D_\alpha$ is the damping of the media. The subscript $\alpha = min, s$ states the minimum value of damping in shear, whereas subscript $\alpha$ ($\alpha$=$s$, $f$) denotes variables associated with solid and fluid, respectively. $D_s$ is the function of uniformity coefficient $C_u$, median grain size $d_{50}$ and mean effective stress $\sigma_0'$, as observed in small-strain dynamic test. The specific expression was recommended in [12] as:

$$D_s = \alpha_0 C_u^{\alpha_1} d_{50}^{\alpha_2} \left(\frac{\sigma_0'}{P_a}\right)^{\alpha_3}, \tag{3}$$

in which $P_a$ is pressure at atmosphere, $\alpha_0$, $\alpha_1$, $\alpha_2$ and $\alpha_3$ are fitting parameters from experiments.

$D_f$ is mainly induced owing to the relative motion of viscous pore fluid with respect to solid, and is found to dependent on moisture content. Therefore, $D_f$ is set to take the following form:

$$D_f = \sum_{i=0}^{=\infty} g_i(S) h_i(\theta_f - \theta_s), \tag{4}$$

where, $S$ is the moisture content, and $\theta_\alpha$ ($\alpha$=$s$, $f$) denotes angular displacement of $\alpha$ component subjected to torsion waves.

In Eq. (4), the first order approximation could be made based on assumption (i)

$$D_f \approx g_0(S) h_0(\theta_f - \theta_s). \tag{5}$$

The $g_0(S)$ would be further expanded into exponential function of $S$, with undetermined coefficients $\eta_j$ and power $\zeta$, as shown in Eq. (6):

$$g_0(S) = \sum_{j=0}^{+\infty} \eta_j (S^\zeta)^j \approx \eta_0 + \eta_1 S^\zeta. \tag{6}$$

The function $h_0(\theta_f - \theta_s)$ is tackled in the similar way with undetermined coefficients $v_k$ and power $\lambda$:

$$h_0\left(\theta_f - \theta_s\right) = \sum_{k=0}^{+\infty} v_k ((\theta_f - \theta_s)^\lambda)^k \approx v_0 + v_1 (\theta_f - \theta_s)^\lambda, \tag{7}$$

in which the term ($\theta_f$ - $\theta_s$) will be deduced below in an analytical manner following Biot theory.

## 3 Analytical Expression of Damping

The governing equation for a saturated poroelastic soil column subjected to rotational wave is given by [13]

$$(1-n)\rho_s \frac{\partial^2 \theta_s}{\partial t^2} = G\frac{\partial^2 \theta_s}{\partial z^2} - \frac{n^2 \rho_f g}{k}\frac{\partial}{\partial t}\left(\theta_s - \theta_f\right) \tag{8-a}$$

$$n\rho_f \frac{\partial^2 \theta_f}{\partial t^2} = \frac{n^2 \rho_f g}{k}\frac{\partial}{\partial t}(\theta_s - \theta_f), \tag{8-b}$$

where $G$ denote the shear modulus of the dry porous frame. The rightmost term denotes the interaction between solid and fluid phases and is canceled out by coupling Eqs. 8(a) and (b). As shown above, the effects of pore pressure are excluded in tortional motion, and the modulus involved is independent on the degree of saturation. Therefore, it is reasonable to consider the effects of saturation degree as a separate correction multiplier in the present model, as illustrated in Eq. (4).

Assuming that the steady-state forced motion varies in a harmonic form $\theta_\alpha = \bar{\theta}_\alpha(z)e^{i\omega t}$ ($\alpha$=*s, f*) with $\omega$ being the circular frequency, inserting Eq. 8(b) into Eq. 8(a) and canceling $\bar{\theta}_s$ lead to

$$\frac{d^2\bar{\theta}_f}{dz^2} = -\frac{\omega^2}{G/\rho'}\bar{\theta}_f \tag{9-a}$$

$$\rho' = \frac{\rho_{sat} - \rho_s \frac{k\omega}{ign}(1-n)}{1-\frac{k\omega}{ign}}. \tag{9-b}$$

The general solutions of Eq. (9) can be written as

$$\bar{\theta}_f = A_1 sin\left(\frac{\omega}{\sqrt{G/\rho'}}z\right) + A_2 cos\left(\frac{\omega}{\sqrt{G/\rho'}}z\right), \tag{10}$$

where the positive $z$-direction is taken downwards with the origin set at top of specimen. The constants $A_1$ and $A_2$ are determined from the boundary conditions in resonant column test, including the loading to the column top and fixed end at the bottom [10]

$$\begin{cases} \left(1-\frac{k\omega}{ign}\right)\left(A_1 GJ\frac{\omega}{\sqrt{G/\rho'}} + A_2 I_t\omega^2\right) = -T_0 \\ \theta_f(H,t) = 0 \end{cases}, \tag{11}$$

where $T_0$ is the torque amplitude, $H$ is the height of specimen, $J$ is polar moment of inertia of soil column and $I_t$ is the mass polar moment of inertia of loading system. Solving Eq. (11) results in

$$\begin{cases} A_1 = \frac{-T_0}{\left(1-\frac{k\omega}{ign}\right)\cdot\left(GJ\frac{\omega}{\sqrt{G/\rho'}} - tan\left(\frac{\omega}{\sqrt{G/\rho'}}H\right)I_t\omega^2\right)} \\ A_2 = \frac{T_0 tan\left(\frac{\omega}{\sqrt{G/\rho'}}H\right)}{\left(1-\frac{k\omega}{ign}\right)\cdot\left(GJ\frac{\omega}{\sqrt{G/\rho'}} - tan\left(\frac{\omega}{\sqrt{G/\rho'}}H\right)I_t\omega^2\right)} \end{cases}. \tag{12}$$

Substituting Eq. (12) into Eq. (10) leads to the fluid rotation in torsional resonance test

$$\overline{\theta_f} = \frac{T_0 H}{GJ} \frac{\cos\left(\frac{\omega z}{\sqrt{G/\rho'}}\right)\tan\left(\frac{\omega H}{\sqrt{G/\rho'}}\right)-\sin\left(\frac{\omega z}{\sqrt{G/\rho'}}\right)}{\left(1-\frac{k\omega}{ign}\right)\cdot\left(\frac{\omega H}{\sqrt{G/\rho'}}-\frac{\omega^2 H^2 I_t}{V_S^2 I}\tan\left(\frac{\omega H}{\sqrt{G/\rho'}}\right)\right)}. \quad (13)$$

The solid displacement can be obtained in the similar manner as shown in [10]. Therefore, the motion of fluid relative to solid can be formulated as

$$\overline{\theta_f} - \overline{\theta_s} = \frac{T_0 H}{GJ}\left(\frac{\cos\left(\frac{\omega z}{\sqrt{G/\rho'}}\right)\tan\left(\frac{\omega H}{\sqrt{G/\rho'}}\right)-\sin\left(\frac{\omega z}{\sqrt{G/\rho'}}\right)}{\left(1-\frac{k\omega}{ign}\right)\left(\frac{\omega H}{\sqrt{G/\rho'}}-\frac{\omega^2 H^2 I_t}{V_S'^2 I}\tan\left(\frac{\omega H}{\sqrt{G/\rho'}}\right)\right)} - \frac{\cos\left(\frac{\omega z}{\alpha V_S}\right)\tan\left(\frac{\omega H}{\alpha V_S}\right)-\sin\left(\frac{\omega z}{\alpha V_S}\right)}{\frac{\omega H}{\alpha V_S}-\frac{\omega^2 H^2 I_t}{V_S^2 I}\tan\left(\frac{\omega H}{\alpha V_S}\right)}\right) \quad (14\text{-a})$$

$$\alpha = \sqrt{\frac{ng+i\omega k}{ng+i(1-n\rho_f/\rho_{sat})\omega k}}, \quad (14\text{-b})$$

in which $I=\rho_{sat}HJ$ is the mass polar moment of inertia of the saturated specimen, $\rho_{sat} = n\rho_f + (1-n)\rho_s$ is the density of saturated soils, $V_s=\sqrt{G/\rho_{sat}}$ is shear wave velocity regardless of relative motion between the two phases. It is evident and reasonable from Eq. (12) that the motion of pore fluid relative to solid vanishes for impermeable soils ($k$=0).

Finally, the total small-strain damping in shear is reformulated as

$$D_{min,s} = \alpha_0 c_u^{\alpha_1} d_{50}^{\alpha_2}\left(\frac{\sigma_0'}{P_a}\right)^{\alpha_3} + (1+\psi_1 S^{\zeta})(\psi_2 + \psi_3 \cdot \mathrm{abs}\left|\overline{\theta_f} - \overline{\theta_s}\right|^{\lambda}), \quad (15)$$

where $\psi_1 = \eta_1/\eta_0$, $\psi_2=\eta_0\nu_0$ and $\psi_3=\eta_0\nu_1$ are to-be-determined parameters in the rearranged form to further reduce one parameter.

# 4 Validations with existing experimental results

## 4.1 Experiment [12]

In this section, parameters in Eq. (15) are first determined by PSO algorithm, followed by comparison of predicted damping with measured one from fixed-free torsion experiments given in [12]. The specimen material is classified as poorly graded gravel (GPM) according to the British Standard Soil Classification System. The soil parameters for different specimens are listed in Table 1. The numbers in brackets stand for different mean effective pressures, and we use A(B/C)-$i$ ($i$=1,2,3) to denote the specific test. The specimens have a diameter of 7.11 cm and height of 14.3 cm, with moisture content of about 6%. The maximum dry density is 2267.2 kg/m$^3$ determined by proctor compaction method. The shear moduli of dry porous material were calculated from the empirical expression fitted in [12]. The ratio of mass polar moment of inertia of loading system to saturated specimen $I_t/I$ is set to one in the fixed-free boundary condition.

Permeability was determined from the modified Kozeny-Carman (KC) equation presented in [14], which is expressed as

$$k = \frac{1}{9\pi^2 k_0}\frac{\rho_f g}{\mu}(d_{50}a \cdot \sin(\frac{\pi}{2a}))^2 \cdot \frac{e^3}{1+e}, \quad (16)$$

in which $\mu$ is dynamic viscosity of pore water, $e$=$n$/(1-$n$) is the void ratio. $a$ is the parameter by fitting with the particle size distribution (PSD), and the PSD for different specimens is depicted in Figure 1. The parameter $k_0$ is the KC constant related to porosity, which is taken to be one herein based on the results in [15].

| Specimen | $d_{50}$/ mm | $C_u$ | $a$ | Moisture content/ % | $n$ | $\rho_{sat}$/ kg·m$^3$ | $G$ / MPa |
|---|---|---|---|---|---|---|---|
| A | 1.48 | 32.7 | 0.459 | 5.6 | 0.19 | 2026.432 | 197.34 (1.25atm), 290.34 (2.25atm), 440.94 (4.25atm) |
| B | 1.48 | 32.7 | 0.427 | 5.5 | 0.20 | 2013.76 | 420.85 (4.25atm) |
| C | 2.12 | 49.7 | 0.426 | 5.9 | 0.19 | 2030.23 | 204.37 (1.25atm), 470.96 (4.25atm) |

Table 1 Soil parameters for different specimens

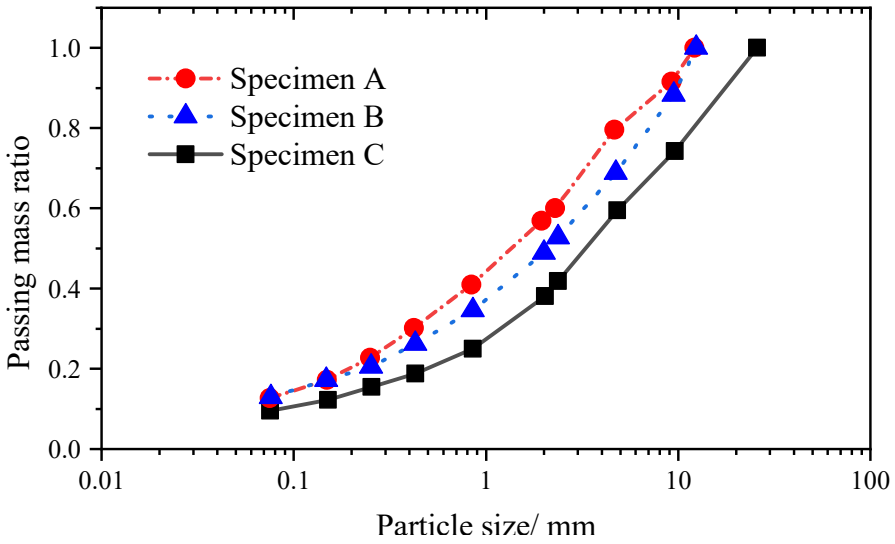


Figure 1 Particle size distribution of three sets of specimens

### 4.2 Validation and discussions

The nine parameters in Eq. (15) were fitted using the data set for specimens A-1, A-3, C-1 and C-2. The collected and fitted results are plotted in Figure 2, marked by solid scatter and dotted line, respectively.

| $\alpha_0$ | $\alpha_1$ | $\alpha_2$ | $\alpha_3$ | $\psi_1$ | $\zeta$ | $\psi_2$ | $\psi_3$ | $\lambda$ |
|---|---|---|---|---|---|---|---|---|
| 7.30 | 0.002 | -2.30 | -0.74 | -24.27 | 9.44 | 0.26 | 17.37 | 0.20 |

Table 2 Fitted parameters in the present damping model

Table 2 summarizes the nine fitted parameters. It is revealed that the increase of $d_{50}$ and $\sigma_0'$ suppresses the skeleton damping, consistent with the findings in [12]. As expected, the hydraulic damping increases with larger relative motions. The predicted damping by the presented model for specimens A-2 and B-1 is illustrated in Figure 3. The slight decrease of measured $D_{\min,s}$ below 1Hz could be attributed to the creeping of soils under such low loading frequency, which is not incorporated in the model. In general, it shows fairly satisfactory agreement between two sets of results.

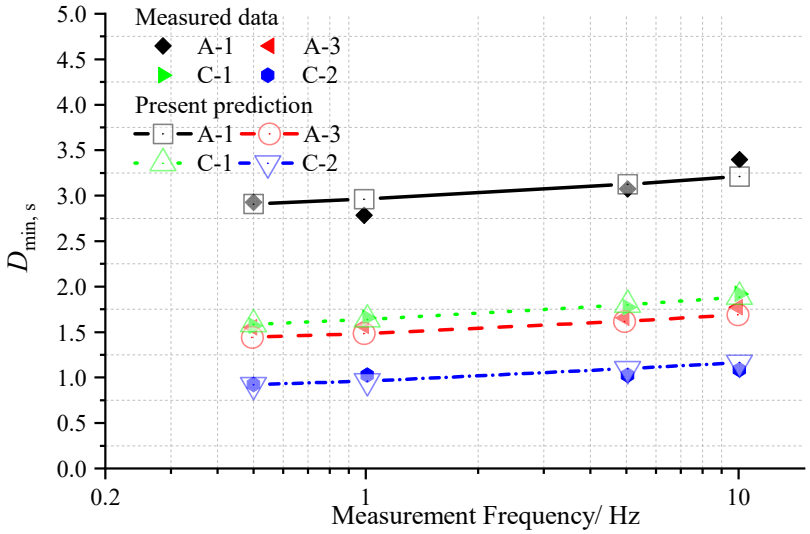


Figure 2 Variation of damping from measured and fitted results versus loading frequency.

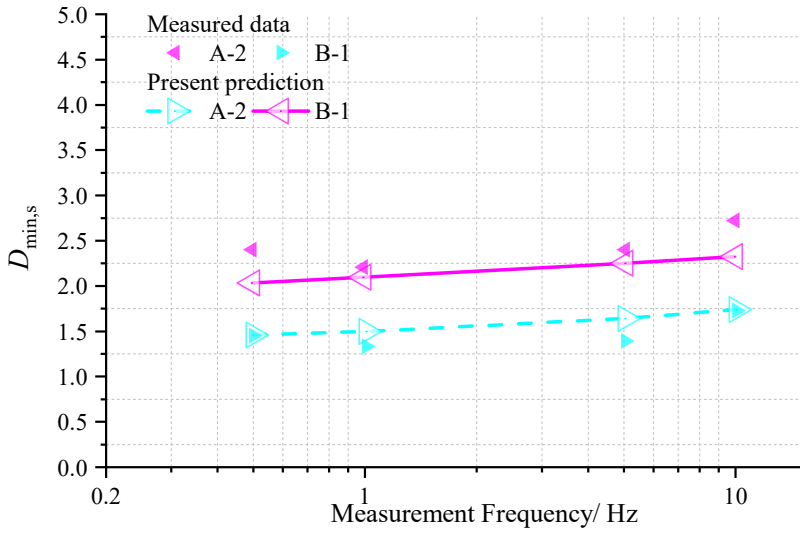


Figure 3 Predicted damping versus loading frequency for specimens A-2 and B-1.

To further investigate the effects of $d_{50}$ on damping of the gravels, the total damping versus frequency is shown in Figure 4 for confining pressures $\sigma_0'$=1.25 and 4.25 atm, respectively. Different values of $d_{50}$=2.12, 4.24, 8.48 and 16.96 mm are used. Permeability varies according to Eq. (16) ($k$=2.46×10$^{-4}$, 9.84×10$^{-4}$, 3.93×10$^{-3}$ and 1.57×10$^{-2}$ m/s), whereas other parameters remain constant as for specimens C-1 and C-2 considering that their variations are influenced by $d_{50}$ much less than does $k$.

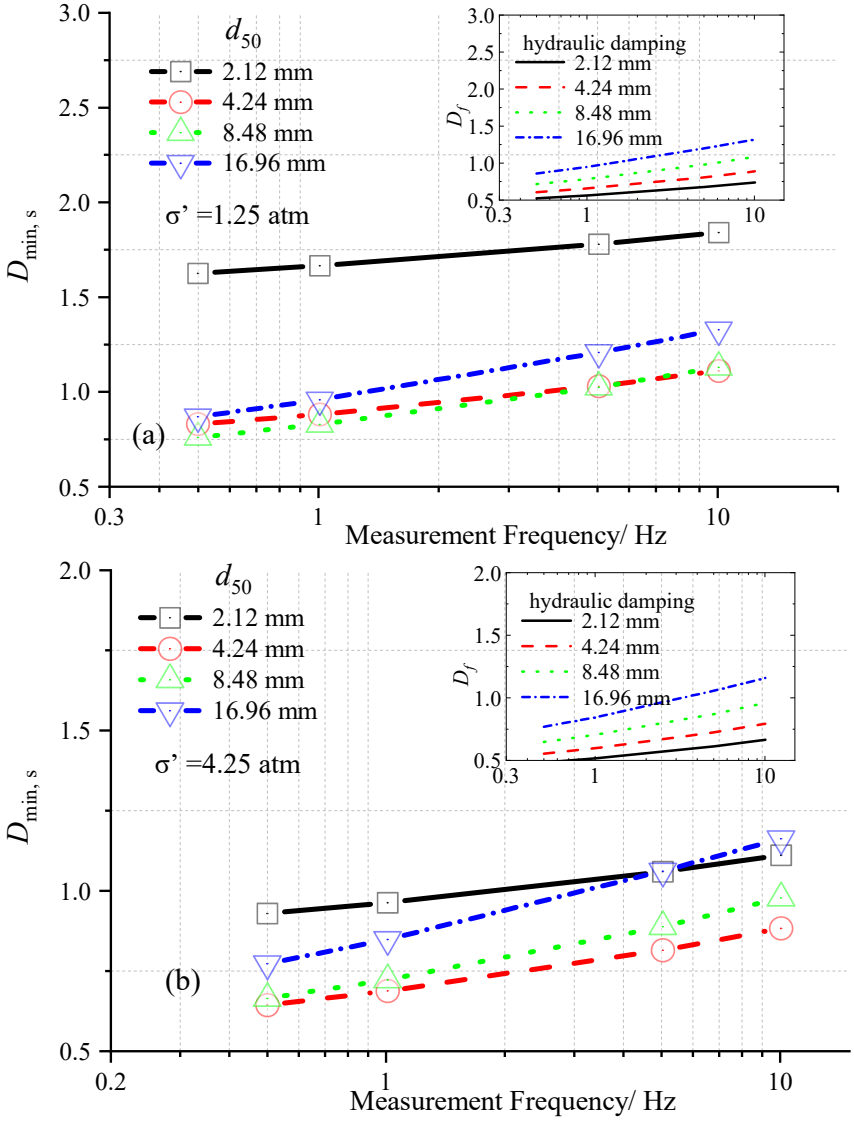


Figure 4 Variation of $D_{min,s}$ versus loading frequency for different values of $d_{50}$ (a) confining pressure $\sigma_0'$=1.25 atm, (b) $\sigma_0'$=4.25 atm.

As can be seen from Figure 4(a) for $\sigma_0'$=1.25 atm, effects of loading frequency tend to be obvious with increasing $d_{50}$. For $d_{50}$=2.12 mm, values of $D_{min,s}$ vary about 10% for frequencies increasing from 0.5 Hz to 10.0 Hz; for $d_{50}$=16.96 mm, however, values of $D_{min,s}$ vary about 50%, illustrating more hydraulic damping for larger $d_{50}$ as shown in the subfigure. The total damping drops by half as $d_{50}$ increases from 2.12 to

8.48mm, and rises for $d_{50}$=16.96mm, this suggests that the effects of $d_{50}$ on hydraulic damping surpass that on the skeleton damping and the viscous motion between two phases is predominant for $d_{50}$=16.96 mm. In Figure 4(b), the hydraulic damping is very close to that for $\sigma_0^{'}$=1.25 atm, while the skeleton damping is remarkably dropped due to higher value of $\sigma_0^{'}$. The total damping rises slightly with $d_{50}$ after the drop for $d_{50}$ increasing from 2.12 to 4.24 mm. This demonstrates that the hydraulic damping cannot be neglected under high confining pressure.

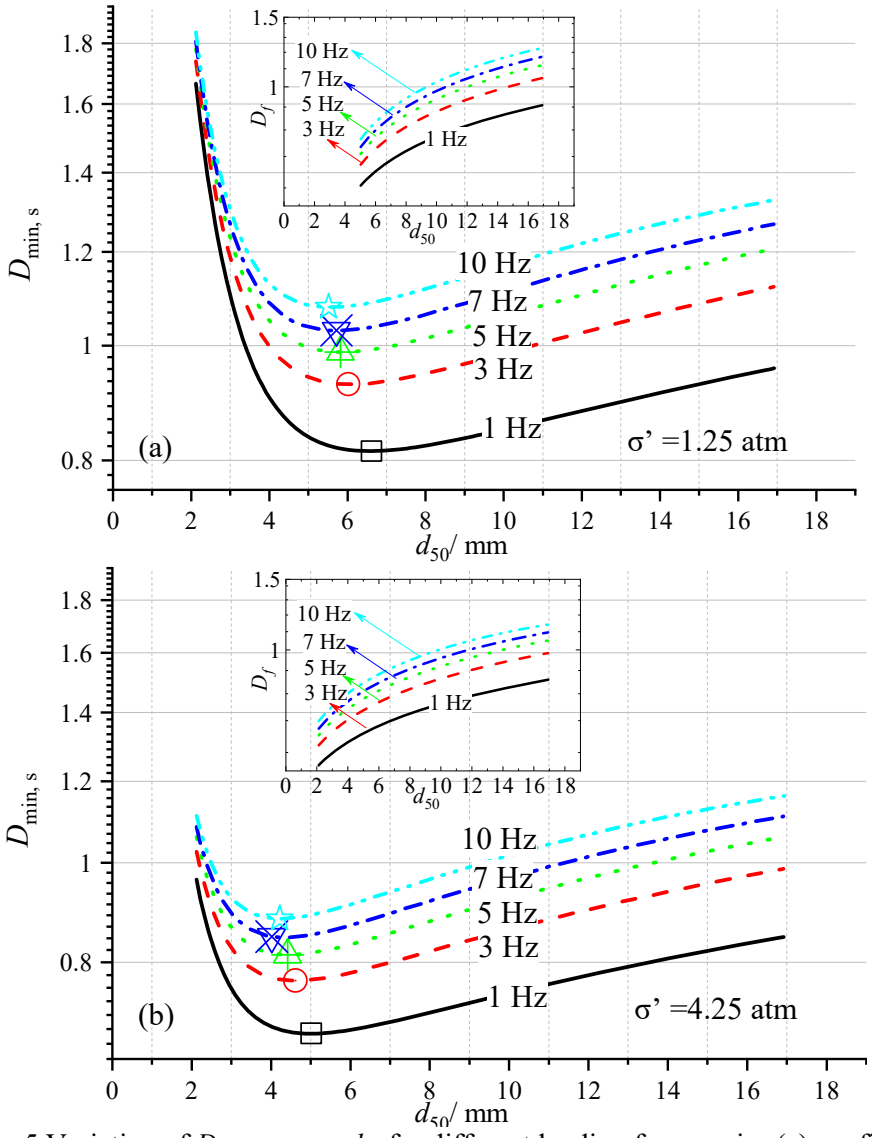


Figure 5 Variation of $D_{min,s}$ versus $d_{50}$ for different loading frequencies (a) confining pressure $\sigma_0^{'}$=1.25 atm, (b) $\sigma_0^{'}$=4.25 atm.

Figure 5 presents the total damping varying with $d_{50}$, with parameters consistent with those in Figure 4. The total damping approximately drops by half at a critical value of $d_{50}$ and increases gradually with increasing $d_{50}$, which could explain the rise of $D_{min,s}$ for coarser gravels in Figure 4. For small values of $d_{50}$, the relative motion is supressed by viscous coupling, thus producing less energy dissipation; however, the

relative motion between two phases is enhanced with larger values of $d_{50}$. The effects of $d_{50}$ on skeleton damping and on hydraulic damping cancel each other out at a critical value of $d_{50}$. Besides, the critical $d_{50}$ is advanced as the loading frequency increases, suggesting more hydraulic damping at high-frequency loadings.

## 5 Conclusions

In this paper, a small-strain damping model in shear for gravelly soil under various loading frequencies was presented. Decomposing the total damping into skeleton damping and hydraulic counterpart, the former was expressed using a classical empirical formulation; while the hydraulic model was proposed within the Biot theory in low frequency part, in which the relative motion between pore fluid and solid was deduced with a fixed-free boundary condition. The fitting parameters in the damping model were evaluated based on the particle swarm optimization algorithm.

The negative correlation between $d_{50}$, $\sigma_0^{'}$ and skeleton damping was revealed from the fitting results, consistent with previous studies. Besides, results showed that the hydraulic damping rises with increasing relative motion between pore fluid and solid as expected. Finally, after comparison of the predicted damping to the measured data for another two specimens, parametric analysis was performed to illustrate the effects of $d_{50}$, $\sigma_0^{'}$ and loading frequency on damping. It was found that effects of loading frequency tend to be obvious with increasing $d_{50}$, the values of $D_{\min,s}$ vary about 50% for frequencies increasing from 0.5 Hz to 10.0 Hz and $\sigma_0^{'}$=1.25 atm. There existed a critical value of $d_{50}$ at which $D_{\min,s}$ takes its minimum value, i.e., the effects of $d_{50}$ on skeleton damping and on hydraulic damping could cancel each other out.

# References


[1] J.P. Bardet, “The damping of saturated poroelastic soils during steady-state vibrations”, Applied Mathematics and Computation, 67, 3–31, 1995, doi: 10.1016/0096-3003(94)00052-6.

[2] F. Jafarzadeh, H. Sadeghi, “Experimental study on dynamic properties of sand with emphasis on the degree of saturation”, Soil Dynamics and Earthquake Engineering, 32, 26–41, 2012, doi: 10.1016/j.soildyn.2011.08.003.

[3] J. Kumar, B.N. Madhusudhan, “Dynamic properties of sand from dry to fully saturated states”, Géotechnique, 62, 45–54, 2012, doi: 10.1680/geot.10.P.042.

[4] B.N. Madhusudhan, J. Kumar, “Damping of Sands for Varying Saturation”, Journal of Geotechnical and Geoenvironmental Engineering, 139, 1625–1630, 2013, doi: 10.1061/(ASCE)GT.1943-5606.0000895.

[5] C. Mancuso, R. Vassallo, A. d’Onofrio, “Small strain behavior of a silty sand in controlled-suction resonant column torsional shear tests”, Canadian Geotechnical Journal, 39, 22–31, 2002, doi: 10.1139/t01-076.

[6] T.T. Dutta, S. Saride, M. Jallu, “Effect of saturation on dynamic properties of compacted clay in a resonant column test”, Geomechanics and Geoengineering, 12, 181–190, 2017, doi: 10.1080/17486025.2016.1208849.

[7] V.C. Xenaki, G.A. Athanasopoulos, “Dynamic properties and liquefaction resistance of two soil materials in an earthfill dam—Laboratory test results”, Soil Dynamics and Earthquake Engineering, 28, 605–620, 2008, doi: 10.1016/j.soildyn.2007.10.001.
[8] G. Kong, H. Li, G. Yang, Z. Cao, “Investigation on shear modulus and damping ratio of transparent soils with different pore fluids”, Granular Matter, 20, 8, 2018, doi: 10.1007/s10035-017-0779-5.
[9] T. Qiu, “Pore Fluid Induced Damping of Saturated Soil in Resonant Column Tests”, in Geotechnical Earthquake Engineering and Soil Dynamics IV, Sacramento, California, United States: American Society of Civil Engineers, 2008, 1–10. doi: 10.1061/40975(318)51.
[10] T. Qiu, P.J. Fox, “Rotation vibration in Biot-Hydraulic Damping of Saturated Poroelastic Soils During Steady-State Vibration”, Journal of Engineering Mechanics, 132, 859–870, 2006, doi: 10.1061/(ASCE)0733-9399(2006)132:8(859).
[11] T. Qiu, Y. Huang, “Analytical and Experimental Studies on Biot Flow–Induced Damping in Saturated Soil Specimens in Resonant Column Tests”, International Journal of Geomechanics, 17, 06017004, 2017, doi: 10.1061/(ASCE)GM.1943-5622.0000915.
[12] F.Y. Menq, “Dynamic properties of sandy and gravelly soils”, Dissertation, The university of Texas at Austin, 2003.
[13] M.A. Biot, “Theory of Propagation of Elastic Waves in a Fluid-Saturated Porous Solid. I. Low-Frequency Range”, The Journal of the Acoustical Society of America, 28, 168–178, 1956, doi: 10.1121/1.1908239.
[14] S. Nomura, Y.Yamamoto, H. Sakaguchi, “Modified expression of Kozeny–Carman equation based on semilog–sigmoid function”, Soils and Foundations, 58, 1350–1357, 2018, doi: 10.1016/j.sandf.2018.07.011.
[15] P. Xu, B. Yu, “Developing a new form of permeability and Kozeny–Carman constant for homogeneous porous media by means of fractal geometry”, Advances in Water Resources, 31, 74–81, 2008, doi: 10.1016/j.advwatres.2007.06.003.